IRIS AperTO

UNIVERSITÀ DEGLI STUDI DI TORINO

AperTO - Archivio Istituzionale Open Access dell'Università di Torino

Combined Effect of Citrate and Fluoride Ions on Hydroxyapatite Nanoparticles

This is the author's manuscript

Original Citation:

Availability:

This version is available http://hdl.handle.net/2318/1743925 since 2020-07-15T10:17:37Z

Published version:

DOI:10.1021/acs.cgd.0c00038

Terms of use:

Open Access

Anyone can freely access the full text of works made available as "Open Access". Works made available under a Creative Commons license can be used according to the terms and conditions of said license. Use of all other works requires consent of the right holder (author or publisher) if not exempted from copyright protection by the applicable law.

(Article begins on next page)

29 July 2024

Combined effect of citrate and fluoride ions on hydroxyapatite nanoparticles

Lorenzo Degli Esposti[a,*], Alessio Adamiano[a], Anna Tampieri[a], Gloria Belen Ramirez-Rodriguez[b], Dritan Siliqi[c], Cinzia Giannini[c], Pavlo Ivanchenko[d], Gianmario Martra[d], Feng-Huei Lin[e,f], José Manuel Delgado-López[b], Michele Iafisco[a,*]

[a]Institute of Science and Technology for Ceramics (ISTEC), National Research Council (CNR), Via Granarolo 64, 48018 Faenza (Italy)

[b]Department of Inorganic Chemistry, University of Granada, Av. Fuente Nueva, s/n, 18071, Granada (Spain)

[c]Institute of Crystallography (IC), National Research Council (CNR), Via Amendola 122/O, 70126 Bari (Italy)

[d]Department of Chemistry and Interdepartmental Centre "Nanostructured Interfaces and Surfaces-NIS", University of Torino, Via P. Giuria 7, 10125, Torino (Italy)

[e]Department of Biomedical Engineering, National Taiwan University, 10617 Taipei (Taiwan)

[f]Institute of Biomedical Engineering and Nanomedicine, National Health Research Institutes, Keyan Road 35, 35053 Miaoli (Taiwan)

Authors for correspondence:

Dr. Michele Iafisco, Ph. D.
Institute of Science and Technology for Ceramics (ISTEC) National Research Council (CNR),
Via Granarolo 64, 48018 Faenza (RA), Italy.
E-mail: michele.iafisco@istec.cnr.it

Lorenzo Degli Esposti, M. Sc.
Institute of Science and Technology for Ceramics (ISTEC) National Research Council (CNR),
Via Granarolo 64, 48018 Faenza (RA), Italy.
E-mail: lorenzo.degliesposti@istec.cnr.it

FT-IR spectra of citrate-HA. The IR-ATR spectra of the citrate-HA samples are reported in Figure S1B. All samples displayed a main broad band at 1030 cm^{-1} with shoulders at 1046 and 1075 cm^{-1} due to the triply degenerated anti-symmetric stretching mode of the apatitic PO_4 groups (ν_3PO_4). Other features emerge at 961 cm^{-1} (symmetric stretching mode of the apatitic PO_4 groups, ν_1PO_4) and at 603, 576 (as a shoulder) and 565 cm^{-1} (triply degenerated bending mode of the same groups, ν_4PO_4). Apatitic hydroxyl groups are evinced by a band at 631 cm^{-1} that is due to OH^- librational modes [1]. The presence of traces amounts of carbonate ions is revealed by the presence of a very weak B-type carbonate substitution (CO_3 occupying PO_4 sites) band at 873 cm^{-1} [2].

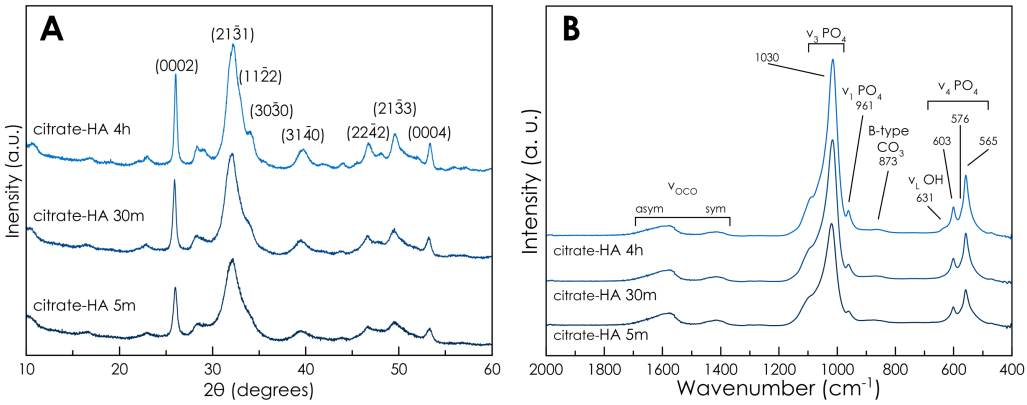

Figure S1. (A) PXRD diffractograms of citrate-HA 5m, citrate-HA 30m, and citrate-HA 4h. (B) FT-IR spectra of citrate-HA 5m, citrate-HA 30m, and citrate-HA 4h.

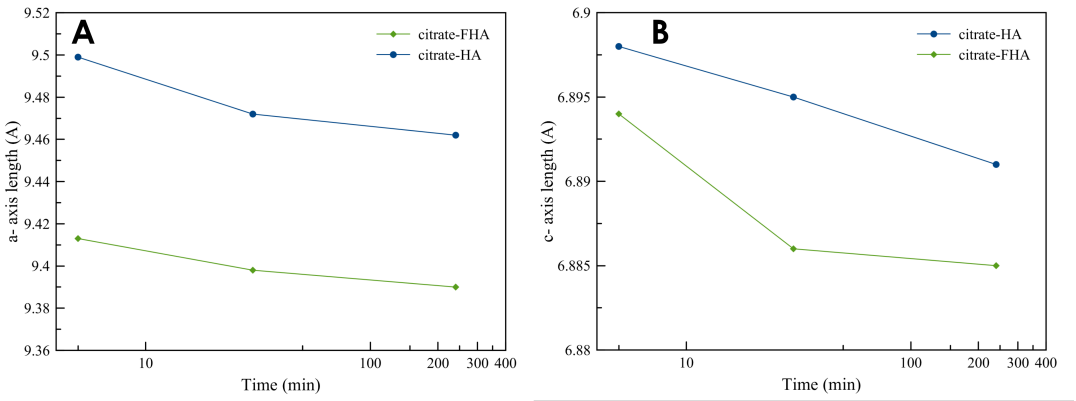

Figure S2. Plot as a function of the maturation time of (A) *a* cell axis, (B) *c* cell axis of citrate-FHA and citrate-HA.

Table S1. Cell parameters and crystal domain of citrate-HA samples.

Sample	*a-b* cell axes (Å)	*c* cell axis (Å)	$D_{(0002)}$ (nm)	$D_{(31-40)}$ (nm)	$D_{(0002)}$/ $D_{(31-40)}$
Citrate-HA 5m	9,499	6,898	21,6±0,5	5.5±0,4	3,9
Citrate-HA 30m	9,472	6,895	28,6±0,5	6,3±0,7	4,3
Citrate-HA 4h	9,462	6,891	42,9±0,5	7.3±0,6	5,9

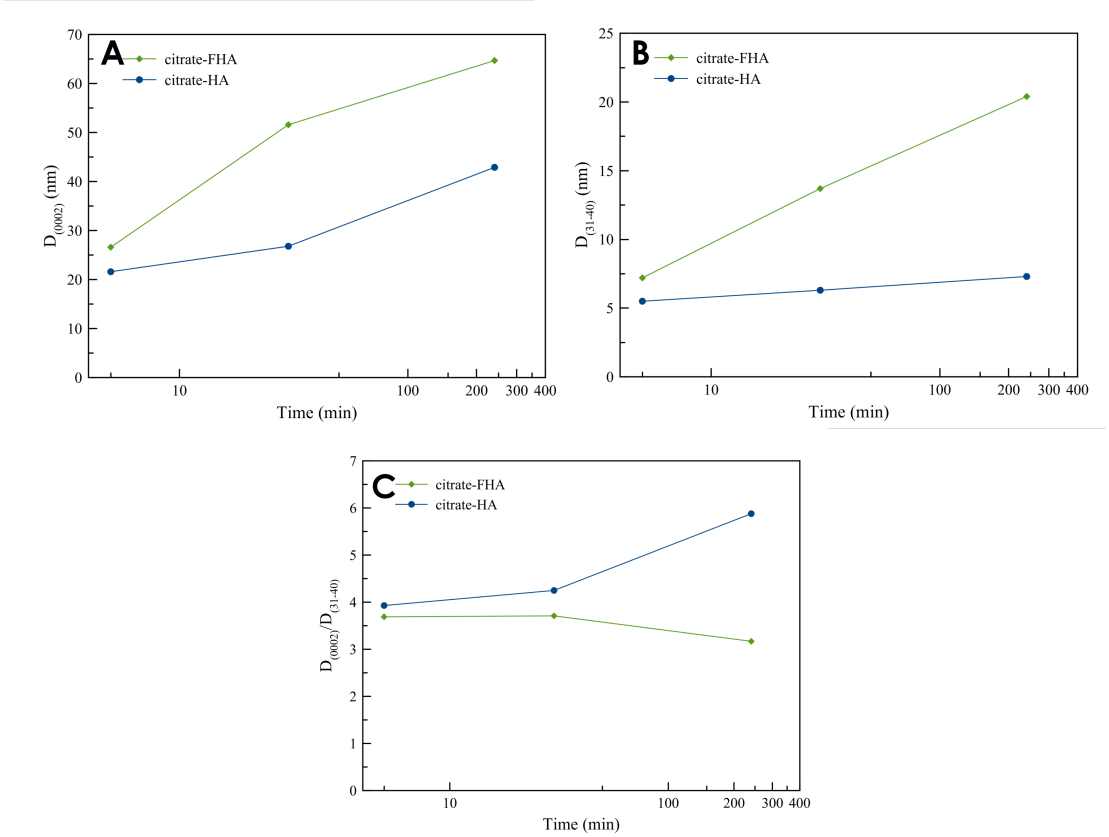

Figure S3. Plot as a function of the maturation time of (A) $D_{(0002)}$ crystal domain, (B) $D_{(31-40)}$ crystal domain and (C) $D_{(0002)}/D_{(31-40)}$ ratio of citrate-FHA and citrate-HA.

Table S2. Chemical composition of citrate-HA samples.

Sample	Ca/P[a] (mol)	F[b] (% wt)	Citrate[c] (% wt)	Carbonate[c] (% wt)	ζ-Potential (mV)
Citrate-HA 5m	1,54±0,02	-	4,8±0,3	1,4±0,2	-13.1 ± 0.4
Citrate-HA 30m	1,54±0,02	-	3,2±0,3	0,8±0,1	-12.4 ± 0.4
Citrate-HA 4h	1,53±0,01	-	2,6±0,2	1,2±0,1	-9.3 ± 0.4

[a]Quantified by ICP-OES; [b]Quantified by fluoride ion electrode; [c]Quantified by TGA.

Thermogravimetric analysis. Thermogravimetric curves and their first derivatives of all the samples mainly shows four weight losses (Figure S4): (i) from room temperature to 200°C due to the adsorbed water, (ii) from 200°C to 400°C related to structural water, (iii) from 400 to 600°C due to the citrate, and (iv) from 600 to 1000°C corresponding to the carbonate ions [3].

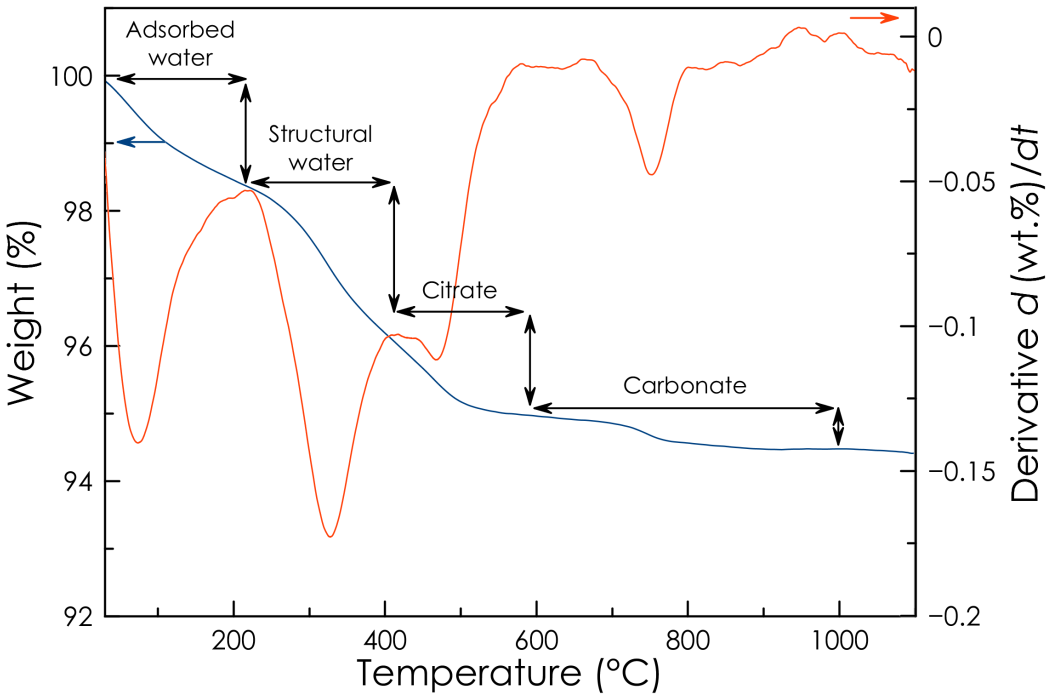

Figure S4. TGA and DTG curve of citrate-FHA 4h. The TGA curves of the other samples have the same profile.

Raman spectroscopy. Figure S5A-B shows the Raman spectra of the samples. The most intense peak appears at 960 cm^{-1}, which corresponds to ν_1PO_4 mode. Other features from apatitic PO_4 group emerge at 1042 cm^{-1} (ν_3PO_4), 586 (ν_4PO_4) and 428 cm^{-1} (ν_2PO_4). In the spectrum of both citrate-FHA and citrate-HA nanoparticles, very weak B-type carbonate bands appeared at 1070 cm^{-1} (ν_1CO_3) and at 1430 cm^{-1} (ν_2CO_3), confirming the data of IR-ATR spectra and chemical analysis [2]. Moreover, the Raman spectrum of citrate-HA samples exhibit an intense peak at 3570 cm^{-1} (Figure S5C-D) associated to the apatitic νOH mode. The intensity of this peak increases with maturation time. On the contrary, this band is not present in the spectrum collected for the citrate-FHA nanoparticles, further confirming that OH^- ions were completely replaced by fluoride ions. The bands at 2930 and 845 cm^{-1} are related to the νCH_2 and the δOCO modes of citrate [4], respectively, and their relative intensity decreases with maturation time as observed in the IR-ATR spectra.

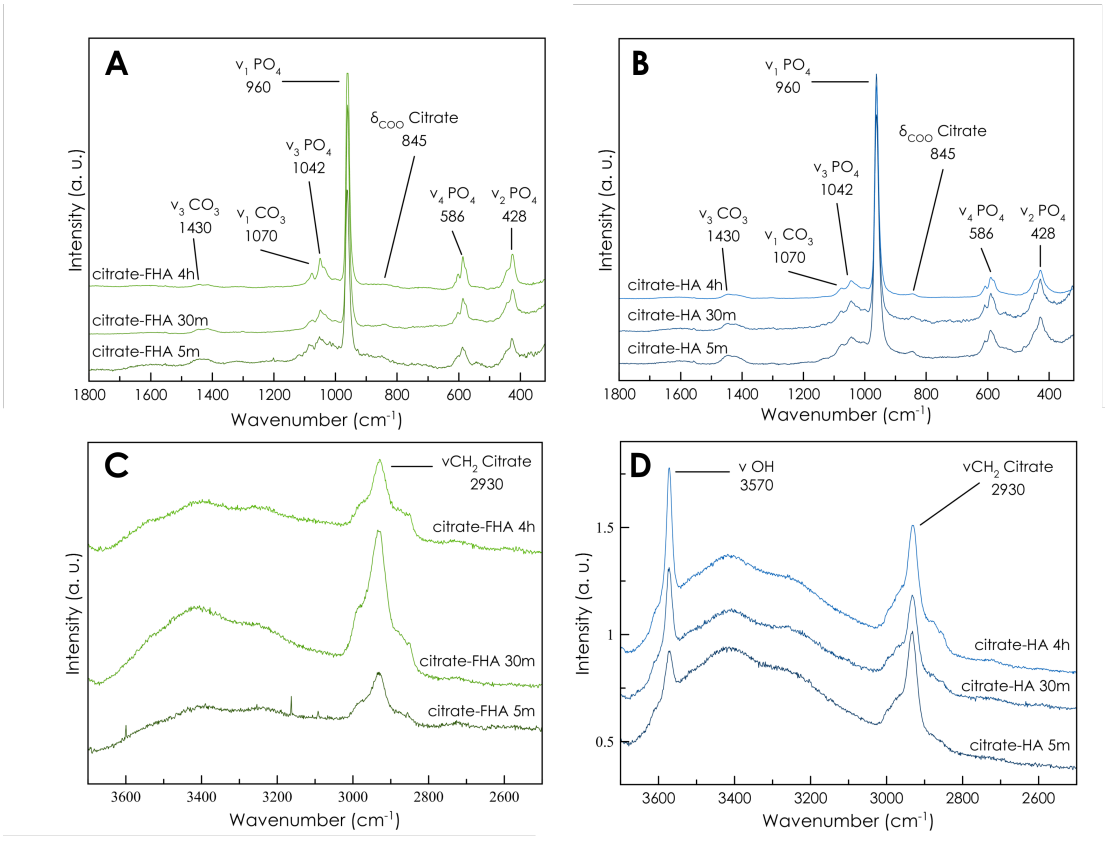

Figure S5. Raman spectra of (A) of citrate-FHA 5m, citrate-FHA 30m, citrate-FHA 4h and (B) citrate-HA 5m, citrate-HA 30m, and citrate-HA 4h. (C) and (D) show an enlarged view of the OH and CH stretching modes spectral region for citrate-FHA and citrate-HA, respectively.

FT-IR spectroscopy in controlled atmosphere mode (Figure S6). The $\nu_{asym}COO$ mode of citrates falling in 1750-1500 cm^{-1} range overlaps with δH_2O mode of adsorbed water (centered at ca. 1645 cm^{-1}). Thus, the detailed analysis of citrate profile requires the complete removal of the adsorbed water. To this aim, the sample in contact with H_2O at 20 mbar (curve a) was outgassed at b.t. for 60 min (curve b). Further, surface-accessible water along with OH species was exchanged with D_2O (δ D_2O is located at 1200 cm^{-1}) by 10 cycles of contacting the sample with 20 mbar of D_2O for 5 min followed by 5 min outgassing with subsequent 60 min outgassing at b.t. (curve c). The resulting profile is 'cleaned' from the contribution of water vibrations in the 1750-1500 cm^{-1} range.

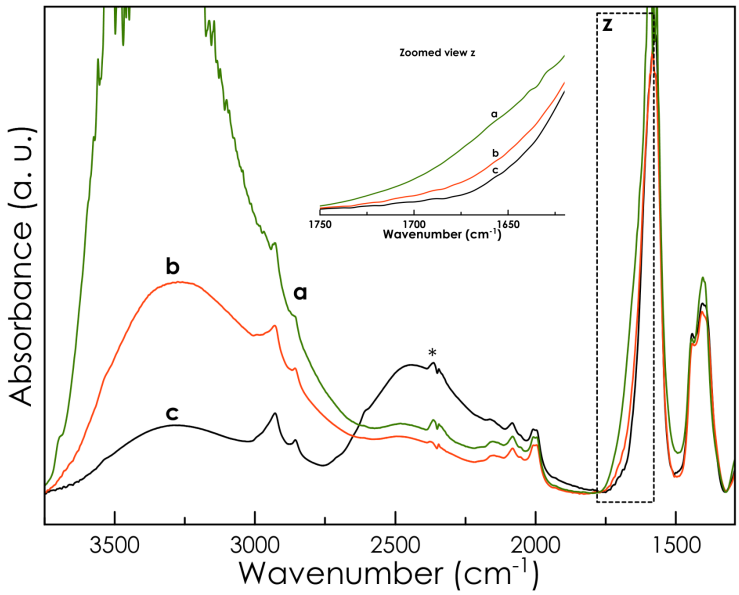

Figure S6. FT-IR spectra of citrate-FHA 4h. Curve (a) in contact with H_2O vapor at 20 mbar; curve (b) after 60 min outgassing at b.t.; curve (c) after exchange with D_2O and subsequent 60 min outgassing at b.t. Inset: zoomed view of 1750-1620 cm^{-1} range. *small feature due to non-compensated atmospheric CO_2.

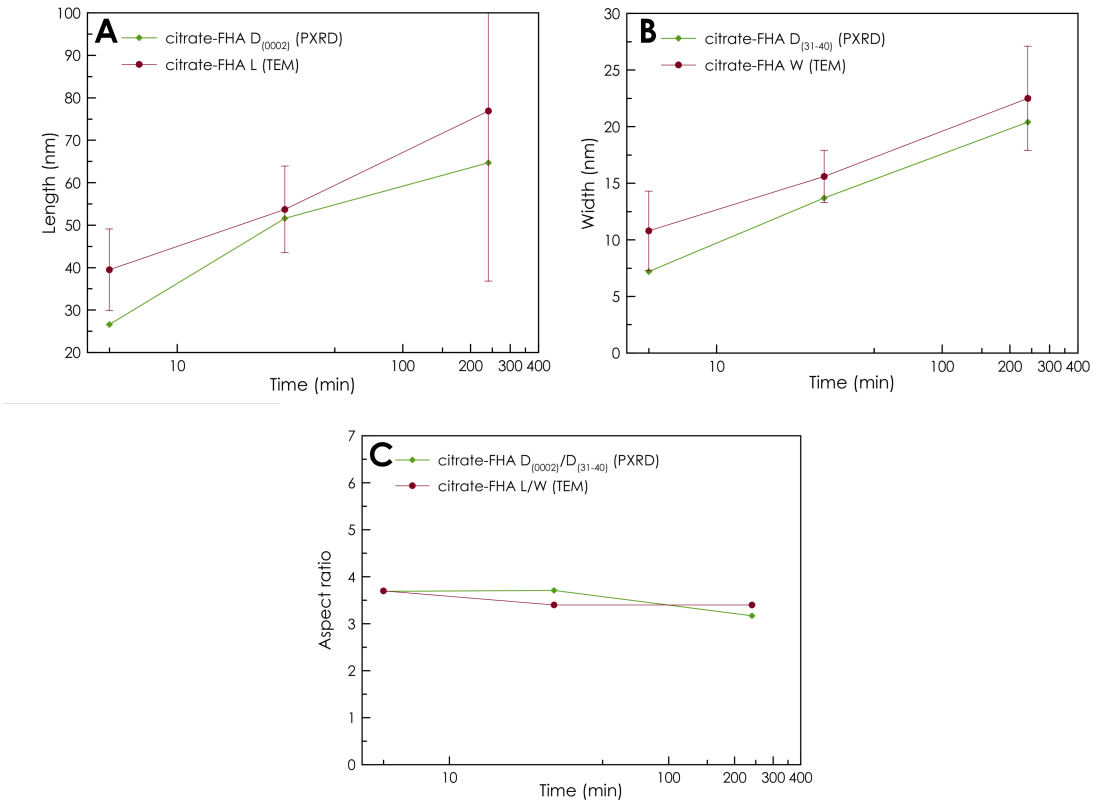

Figure S7. Plot as a function of the maturation time of (A) length, (B) width, and (C) aspect ratio of citrate-FHA nanoparticles evaluated by TEM. A comparison with the respective crystal domains calculated by PXRD patterns is reported in each panel.

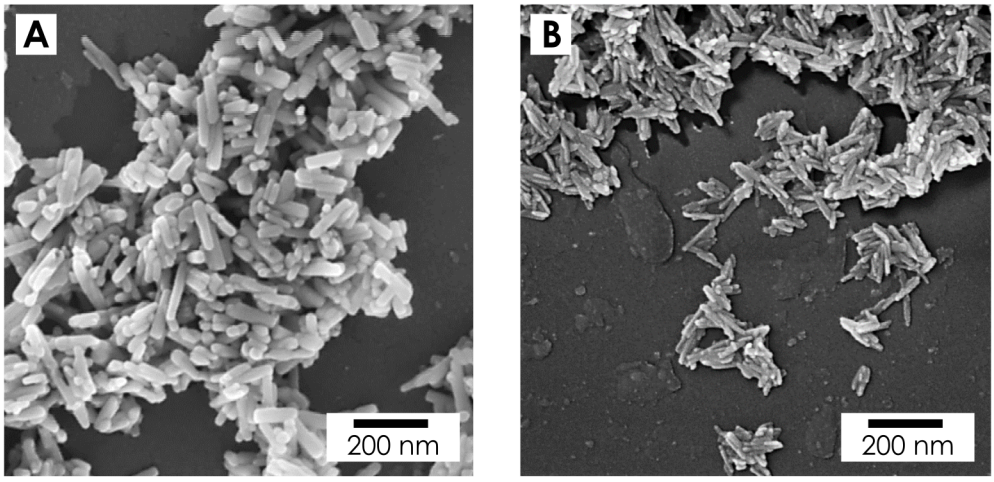

Figure S8. FEG-SEM micrographs of (A) citrate-FHA 4h, and (B) citrate-HA 4h.

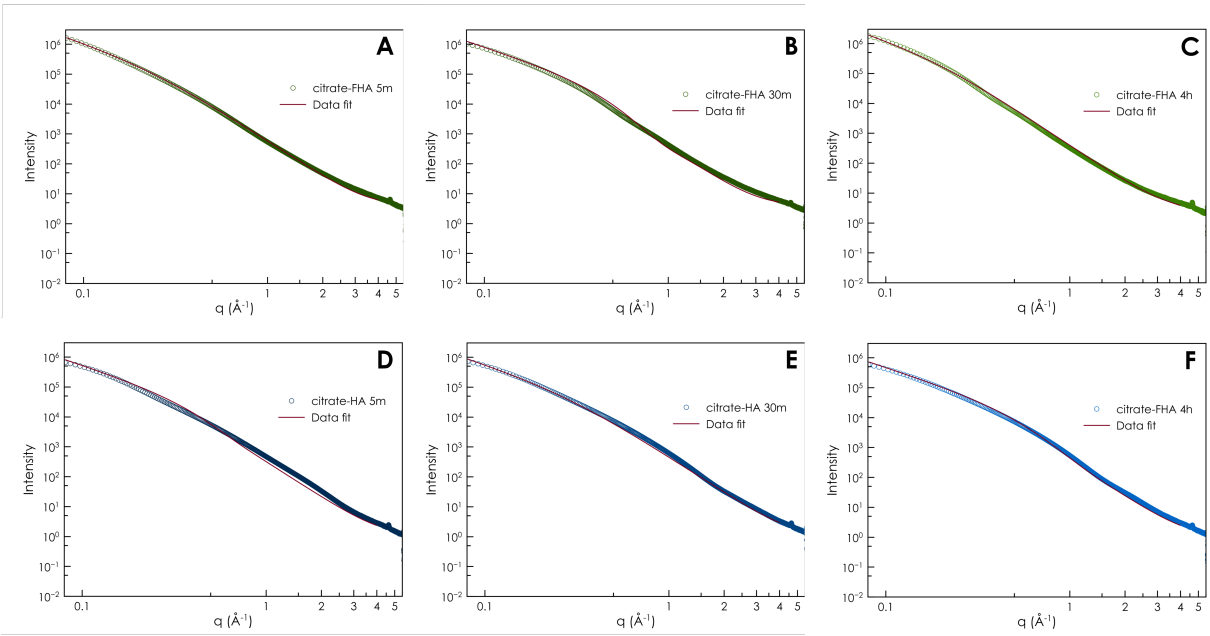

Figure S9. SAXS curves and data fitting with lamellar model for (A) of citrate-FHA 5m, (B) citrate-FHA 30m, (C) citrate-FHA 4h, (D) of citrate-HA 5m, (E) citrate-HA 30m, and (F) citrate-HA 4h.

Table S3. Mean thickness and polydispersity of citrate-HA samples extracted as lamellar model fitting SAXS data.

Sample	Thickness (nm)	Polydispersity
Citrate-HA 5m	6,8	0,47
Citrate-HA 30m	7,1	0,70
Citrate-HA 4h	5,5	0,30

References

1. Koutsopoulos, S., *Synthesis and characterization of hydroxyapatite crystals: a review study on the analytical methods.* Journal of Biomedical Materials Research: An Official Journal of The Society for Biomaterials, The Japanese Society for Biomaterials, and The Australian Society for Biomaterials and the Korean Society for Biomaterials, 2002. **62**(4): p. 600-612.
2. Antonakos, A., E. Liarokapis, and T. Leventouri, *Micro-Raman and FTIR studies of synthetic and natural apatites.* Biomaterials, 2007. **28**(19): p. 3043-3054.
3. Tonsuaadu, K., et al., *A review on the thermal stability of calcium apatites.* Journal of Thermal Analysis and Calorimetry, 2011. **110**(2): p. 647-659.
4. Socrates, G., *Infrared and Raman characteristic group frequencies: tables and charts*. 2004: John Wiley & Sons.